INTERNATIONAL JOURNAL FOR NUMERICAL METHODS IN ENGINEERING
*Int. J. Numer. Meth. Engng* 2005; **63**:1069–1088
Published online 17 March 2005 in Wiley InterScience (www.interscience.wiley.com). DOI: 10.1002/nme.1314

# A new discontinuous upper bound limit analysis formulation

Kristian Krabbenhoft, Andrei V. Lyamin, Mohammed Hjiaj and Scott W. Sloan*, †

*Department of Civil, Surveying and Environmental Engineering, University of Newcastle, NSW 2308, Australia*

SUMMARY

A new upper bound formulation of limit analysis of two- and three-dimensional solids is presented. In contrast to most discrete upper bound methods the present one is formulated in terms of stresses rather than velocities and plastic multipliers. However, by means of duality theory it is shown that the formulation does indeed result in rigorous upper bound solutions. Also, kinematically admissible discontinuities, which have previously been shown to be very efficient, are given an interpretation in terms of stresses. This allows for a much simpler implementation and, in contrast to existing formulations, extension to arbitrary yield criteria in two and three dimensions is straightforward. Finally, the capabilities of the new method are demonstrated through a number of examples. Copyright © 2005 John Wiley & Sons, Ltd.

KEY WORDS: limit analysis; plasticity; duality; upper bound; discontinuous; finite element

## 1. INTRODUCTION

The mathematical theory of plasticity provides two theorems for the determination of the ultimate load of a body of perfectly plastic material. The lower bound theorem states that if, for a given set of loads, an equilibrium stress field can be found, which nowhere violates the yield criterion, the body will not collapse. The upper bound theorem states that, for a given collapse mechanism whose strain rate field complies with the appropriate associated flow rule, the ratio between the internal and external rates of dissipation will be higher than or equal to that actually found at collapse, thus providing an upper bound on the ultimate load.

The duality between these two theorems is well-established, see e.g. References [1, 2]. In the lower bound method one operates with stresses and a load multiplier, whereas the upper bound method involves velocities and plastic multipliers. The variables of the two problems are coupled by the flow rule stating that the strain rate vector is proportional to the gradient of the yield function, and by the condition that the plastic multipliers can be non-negative only at points where the yield function is equal to zero.

*Correspondence to: S. W. Sloan, Department of Civil, Surveying and Environmental Engineering, University of Newcastle, NSW 2308, Australia.
†E-mail: scott.sloan@newcastle.edu.au

*Received 27 February 2004*
*Revised 5 January 2005*
*Accepted 12 January 2005*

This mechanical duality has an analogy in the duality of mathematical programming. Here it is equally well-established that any convex optimization problem has a dual counterpart whose variables are different from those of the original (primal) problem but whose solution, in terms of the optimal value of the objective function, is identical to that of the primal problem.

These duality properties were exploited by Anderheggen and Knöpfel [3] to introduce two approaches to numerical limit analysis namely the '$\alpha\rightarrow$ max method' and the '$\alpha\rightarrow$ min method'. The $\alpha\rightarrow$ max method takes the form of a lower bound type problem where a load factor $\alpha$ is maximized subject to equilibrium and yield constraints. The $\alpha\rightarrow$ min problem, on the other hand, has the form of a typical upper bound problem where the internal rate of dissipation, i.e. $\alpha$, is minimized subject to compatibility constraints. In addition, a constraint limiting the magnitude of the external dissipation to unity is imposed so that $\alpha$ can be seen as a load multiplier as in the $\alpha\rightarrow$ max problem.

Depending on how the equilibrium/compatibility constraints of the two problems are set up, both methods have the capability of producing rigorous bounds on the exact value of $\alpha$. Obviously, if the equilibrium equations are formulated such as to satisfy equilibrium exactly, the $\alpha\rightarrow$ max problem will result in a true lower bound solution, and conversely, if all compatibility requirements are met in the $\alpha\rightarrow$ min problem the solution will be an upper bound. It is, however, also possible to formulate $\alpha\rightarrow$ max problems whose solutions are upper bounds and vice versa for the $\alpha\rightarrow$ min problem. In this case the dual of either problem should comply with the necessary requirements, e.g. the dual of the $\alpha\rightarrow$ max problem should meet all the requirements of the upper bound theorem. Finally, there are two other possibilities: neither the original primal problem nor the dual fulfil the respective requirements or both the primal and the dual problem fulfil the respective requirements. The former scenario usually results from mixed discretizations and will lead to solutions whose bounds cannot be identified, whereas in the latter case the exact solution will result (such discretizations are possible for bars and beams loaded by point forces).

In the following we focus on the upper bound $\alpha\rightarrow$ max approach, i.e. formulations which involve linear equilibrium and linear and/or non-linear yield constraints and lead to upper bounds on the true solution. Compared to the traditional formulations of the upper bound theorem this approach has several advantages. From an implementation point of view, a much more convenient formulation is achieved. This formulation is easily generalized to arbitrary yield criteria and the inclusion of kinematically admissible velocity discontinuities does not create any particular difficulties. The extension to three dimensions, again with arbitrary yield criteria, is also straightforward.

## 2. STRESS-BASED UPPER BOUND OPTIMIZATION PROBLEM

For plates loaded in their own plane, Anderheggen and Knöpfel [3] showed that upper bound solutions can be computed by a triangular constant stress–linear velocity element, see Figure 1, provided that the weak form of the equilibrium conditions are imposed in the $\alpha\rightarrow$ max problem. For discussion of general mixed elements we refer to Borges *et al*. [4].

The basic equations of static equilibrium are given by

$$\mathbf{L}^{\mathsf{T}}\boldsymbol{\sigma}+\rho\mathbf{g}=\mathbf{0} \tag{1}$$

 

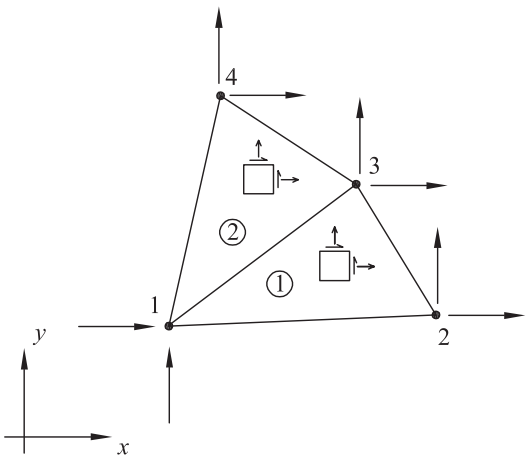


Figure 1. Mesh of constant stress–linear velocity elements.

where $\boldsymbol{\sigma} = (\sigma_x, \sigma_y, \tau_{xy})^{\mathsf{T}}$ is the stress vector, $\rho\mathbf{g}$ is the body force and $\mathbf{L}$ is a matrix of linear differential operators. For a two-dimensional continuum $\mathbf{L}$ is given by

$$\mathbf{L}^{\mathsf{T}} = \begin{bmatrix} \partial/\partial x & 0 & \partial/\partial y \\ 0 & \partial/\partial y & \partial/\partial x \end{bmatrix} \tag{2}$$

The weak form of the equilibrium equations (1) can be written as

$$\int_A \dot{\mathbf{u}}^{\mathsf{T}} \mathbf{L}^{\mathsf{T}} \boldsymbol{\sigma} \, \mathrm{d}A - \int_A \dot{\mathbf{u}}^{\mathsf{T}} \rho \mathbf{g} \, \mathrm{d}A - \int_S \dot{\mathbf{u}}^{\mathsf{T}} \mathbf{t} \, \mathrm{d}S = 0 \tag{3}$$

where $\dot{\mathbf{u}} = (\dot{u}_x, \dot{u}_y)^{\mathsf{T}}$ is the velocity vector, $\mathbf{t} = (t_x, t_y)^{\mathsf{T}}$ the traction vector acting on the boundary $S$, and $A$ the area (here and in the following we assume a unit thickness). We note that the strain rates are given by

$$\dot{\boldsymbol{\varepsilon}} = \begin{bmatrix} \dot{\varepsilon}_x \\ \dot{\varepsilon}_y \\ \dot{\gamma}_{xy} \end{bmatrix} = \mathbf{L}\dot{\mathbf{u}} \tag{4}$$

Within each element the velocity fields are now approximated as

$$\dot{\mathbf{u}}(x, y) = \mathbf{N}(x, y)\dot{\mathbf{a}} \tag{5}$$

where $\mathbf{N}$ contains the interpolation functions and $\dot{\mathbf{a}}$ the nodal velocities.

Inserting the velocity approximation (5) into (3) we get the matrix form of the equilibrium equations as

$$\mathbf{B}^{\mathsf{T}}\boldsymbol{\sigma} = \mathbf{p} \tag{6}$$

 

where

$$\mathbf{B} = \int_A \mathbf{L}\mathbf{N}\,\mathrm{d}A = A\mathbf{L}\mathbf{N} \tag{7}$$

and

$$\mathbf{p} = \int_A \mathbf{N}^{\mathsf{T}}\rho\mathbf{g}\,\mathrm{d}A + \int_S \mathbf{N}^{\mathsf{T}}\mathbf{t}\,\mathrm{d}S \tag{8}$$

Using this weak form of the equilibrium equations, a load optimization problem may now be formulated as

$$\begin{aligned} &\text{maximize} && \alpha \\ &\text{subject to} && \mathbf{B}^{\mathsf{T}}\boldsymbol{\sigma} = \alpha\mathbf{p} \\ & && \mathbf{f}(\boldsymbol{\sigma}) \leqslant 0 \end{aligned} \tag{9}$$

where $\mathbf{p}$ is a set of predefined external loads and $\mathbf{f}$ defines the yield conditions.

## 3. VELOCITY-BASED UPPER BOUND OPTIMIZATION PROBLEM

As stated earlier the $\alpha \rightarrow$ max problem (9) will in fact result in upper bounds on the load multiplier. To show this the dual to (9) is derived. First, a linearization of the non-linear yield conditions about points $\boldsymbol{\sigma}^*$ lying on the yield surface is considered. The yield function then reads

$$\mathbf{f}(\boldsymbol{\sigma}) \simeq \mathbf{f}(\boldsymbol{\sigma}^*) + \nabla\mathbf{f}^{\mathsf{T}}(\boldsymbol{\sigma} - \boldsymbol{\sigma}^*) = \nabla\mathbf{f}^{\mathsf{T}}(\boldsymbol{\sigma} - \boldsymbol{\sigma}^*) \tag{10}$$

where the last equality follows from the fact that $\mathbf{f}(\boldsymbol{\sigma}^*) = \mathbf{0}$. The linearized $\alpha \rightarrow$ max problem is then given by

$$\begin{aligned} &\text{maximize} && \alpha \\ &\text{subject to} && \mathbf{B}^{\mathsf{T}}\boldsymbol{\sigma} = \alpha\mathbf{p} \\ & && \nabla\mathbf{f}^{\mathsf{T}}\boldsymbol{\sigma} \leqslant \nabla\mathbf{f}^{\mathsf{T}}\boldsymbol{\sigma}^* \end{aligned} \tag{11}$$

The dual to this problem is given by, see e.g. Reference [5],

$$\begin{aligned} &\text{minimize} && (\nabla\mathbf{f}\dot{\bar{\boldsymbol{\lambda}}})^{\mathsf{T}}\boldsymbol{\sigma}^* \\ &\text{subject to} && \mathbf{B}\dot{\mathbf{u}} = \nabla\mathbf{f}\dot{\bar{\boldsymbol{\lambda}}} \\ & && \mathbf{p}^{\mathsf{T}}\dot{\mathbf{u}} = 1 \\ & && \dot{\bar{\boldsymbol{\lambda}}} \geqslant \mathbf{0} \end{aligned} \tag{12}$$

This corresponds to a classical upper bound problem and can be interpreted as follows. The plastic strain rates are derived from the yield function by using an associated flow rule of the form

$$\dot{\bar{\boldsymbol{\varepsilon}}} = \dot{\boldsymbol{\varepsilon}}A = \mathbf{B}\dot{\mathbf{u}} = \nabla\mathbf{f}\dot{\boldsymbol{\lambda}}A = \nabla\mathbf{f}\dot{\bar{\boldsymbol{\lambda}}} \tag{13}$$

 

where $\dot{\mathbf{u}}$ are interpreted as the velocities and $\dot{\bar{\boldsymbol{\lambda}}}$ as the plastic multipliers times the area of the triangle, cf. (4) and (7). Since the strain rate fields are constant, the flow rule needs only to be imposed once in each element.

The internal rate of dissipation is given by

$$\dot{D}_{\mathrm{i}} = \int_V \dot{\boldsymbol{\varepsilon}}^{\mathsf{T}} \boldsymbol{\sigma}^* \, \mathrm{d}V = (\nabla \mathbf{f} \dot{\bar{\boldsymbol{\lambda}}})^{\mathsf{T}} \boldsymbol{\sigma}^* \tag{14}$$

which is identical to the objective function in (12).

Furthermore, we limit the magnitude of the external dissipation to unity, i.e.

$$\dot{D}_{\mathrm{e}} = \mathbf{p}^{\mathsf{T}} \dot{\mathbf{u}} = 1 \tag{15}$$

Finally, the plastic multipliers must be positive as expressed by the last set of restrictions in (12). Therefore, regardless of whether we start by setting up the $\alpha \rightarrow$ max problem (9), or its dual the $\alpha \rightarrow$ min problem (12), the result will be a rigorous upper bound on the true collapse multiplier.

## 4. INCLUDING DISCONTINUITIES

The constant stress–linear velocity triangle, also known in displacement finite element analysis as the constant strain triangle, is known to be prone to locking under plastic flow in plane strain and general three-dimensional states of stress. The classical remedy to this problem is to arrange the elements in a special mesh pattern, e.g. consisting of quadrilateral patches each comprising four triangular elements [6]. Recently, several other methods have been explored by de Borst and co-workers, see Reference [7] and references therein. These include the use of selective integration, the so-called B-bar method, enhanced assumed strains, and local higher order polynomial enrichment of nodes undergoing plastic flow. All these methods, however, have their limitations, and it seems that the only really general and robust way of overcoming the locking phenomenon for displacement finite elements in elasto–plastic computations is the use of higher order displacement models as originally suggested by Sloan and Randolph [8].

An alternative approach, which was introduced by Sloan and Kleeman [9] for the purpose of upper bound limit analysis using the Mohr–Coulomb yield criterion, is to include the possibility of kinematically admissible discontinuities between the elements. This approach proved very successful in that no special arrangement of the grid was necessary to overcome locking. Recently, the scheme has been generalized to three-dimensional Mohr–Coulomb plasticity by Lyamin and Sloan [10], where similar advantages are seen.

In the original formulation [9] linear velocity triangles were used and the plastic multipliers were assumed constant, see Figure 2. If the material parameters are uniform over each triangle, these constant plastic multiplier fields correspond to constant stress fields in the dual problems. The velocity jumps between the elements in Reference [9] were constrained to comply with the appropriate flow rule, and the total internal rate of dissipation, i.e. comprising contributions from both the triangular elements and the discontinuities, was minimized in an $\alpha \rightarrow$ min type problem similar to (12).

In the following we will show that the dual problem is one which consists of an assembly of triangular elements connected at the nodes by a two-element patch of infinitely thin elements, see Figure 3.

 

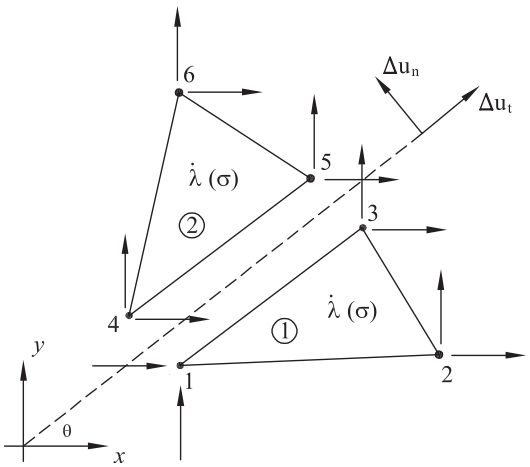


Figure 2. Mesh of constant stress–linear discontinuous velocity elements.

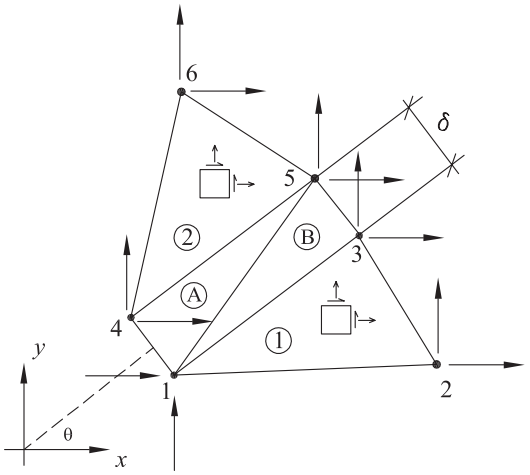


Figure 3. Interpretation of discontinuous upper bound formulation in terms of stresses.

### *4.1. Weak discontinuity equilibrium*

Consider the patch of interconnecting infinitely thin elements shown in Figure 4. We define the stresses and the velocities in a local $t$–$n$ co-ordinate system as shown in the figure.

The velocities in triangle $A$ are taken to vary as

$$\begin{aligned} \dot{u}_t &= \xi_1 \dot{u}_t^1 + \xi_5 \dot{u}_t^5 + \xi_4 \dot{u}_t^4 \\ \dot{u}_n &= \xi_1 \dot{u}_n^1 + \xi_5 \dot{u}_n^5 + \xi_4 \dot{u}_n^4 \end{aligned} \tag{16}$$

 

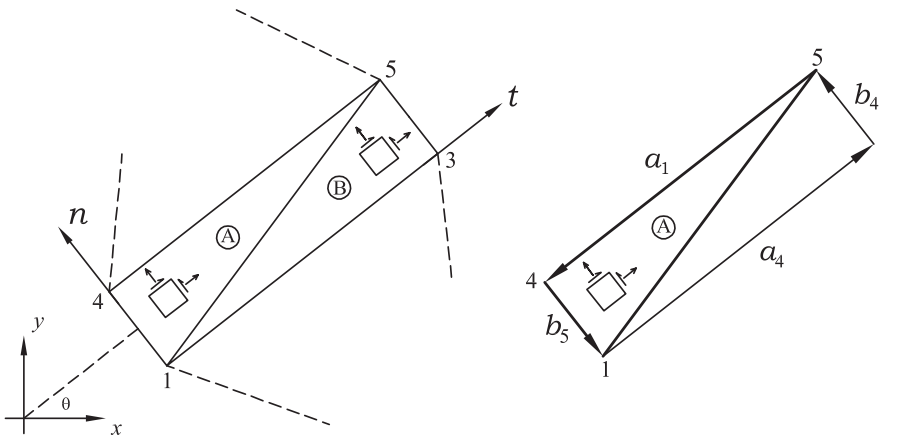


Figure 4. Interpretation of velocity discontinuities in terms of stresses.

where $\xi_j$ are the standard area co-ordinates, see e.g. Reference [11]. Differentiating these relations, the plastic strain rates are computed as

$$\dot{\varepsilon}_t = \frac{1}{A}\dot{\bar{\varepsilon}}_t = \frac{\partial \dot{u}_t}{\partial t} = -\frac{1}{2A}(b_1\dot{u}_t^1 + b_5\dot{u}_t^5 + b_4\dot{u}_t^4) \tag{17}$$

$$\dot{\varepsilon}_n = \frac{1}{A}\dot{\bar{\varepsilon}}_n = \frac{\partial \dot{u}_n}{\partial n} = \frac{1}{2A}(a_1\dot{u}_n^1 + a_5\dot{u}_n^5 + a_4\dot{u}_n^4) \tag{18}$$

$$\dot{\gamma}_{tn} = \frac{1}{A}\dot{\bar{\gamma}}_{tn} = \frac{\partial \dot{u}_t}{\partial n} + \frac{\partial \dot{u}_n}{\partial t} = -\frac{1}{2A}(b_1\dot{u}_n^1 + b_5\dot{u}_n^5 + b_4\dot{u}_n^4) + \frac{1}{2A}(a_1\dot{u}_t^1 + a_5\dot{u}_t^5 + a_4\dot{u}_t^4) \tag{19}$$

In the limit of $\delta \to 0$, which corresponds to a zero-thickness discontinuity, we have

$$b_4 = b_5 = \delta \to 0 \tag{20}$$

Since $a_4 = -a_1 = L$, the strain rates multiplied by the element area become

$$\dot{\bar{\varepsilon}}_t = \tfrac{1}{2}\delta(\dot{u}_t^5 - \dot{u}_t^4) = 0 \tag{21}$$

$$\dot{\bar{\varepsilon}}_n = \tfrac{1}{2}L(\dot{u}_n^4 - \dot{u}_n^1) = \tfrac{1}{2}L\Delta\dot{u}_n^A \tag{22}$$

$$\dot{\bar{\gamma}}_{tn} = \tfrac{1}{2}L(\dot{u}_t^4 - \dot{u}_t^1) = \tfrac{1}{2}L\Delta\dot{u}_t^A \tag{23}$$

 

Similarly, for triangle $B$ we get

$$\dot{\bar{\varepsilon}}_t = \tfrac{1}{2}\delta(\dot{u}_t^3 - \dot{u}_t^1) = 0 \tag{24}$$

$$\dot{\bar{\varepsilon}}_n = \tfrac{1}{2}L(\dot{u}_n^5 - \dot{u}_n^3) = \tfrac{1}{2}L\Delta\dot{u}_n^B \tag{25}$$

$$\dot{\bar{\gamma}}_{tn} = \tfrac{1}{2}L(\dot{u}_t^5 - \dot{u}_t^3) = \tfrac{1}{2}L\Delta\dot{u}_t^A \tag{26}$$

The internal dissipation in the discontinuity is then given by

$$\begin{aligned}\dot{D}_{\mathrm{i}}^{\mathrm{d}} &= \int_{V_A} \boldsymbol{\sigma}_A^{\mathsf{T}}\dot{\boldsymbol{\varepsilon}}_A \,\mathrm{d}V + \int_{V_B} \boldsymbol{\sigma}_B^{\mathsf{T}}\dot{\boldsymbol{\varepsilon}}_B \,\mathrm{d}V = \boldsymbol{\sigma}_A^{\mathsf{T}}\dot{\bar{\boldsymbol{\varepsilon}}}_A + \boldsymbol{\sigma}_B^{\mathsf{T}}\dot{\bar{\boldsymbol{\varepsilon}}}_B \\ &= \tfrac{1}{2}L(\sigma_n^A\Delta\dot{u}_n^A + \tau_{tn}^A\Delta\dot{u}_t^A + \sigma_n^B\Delta\dot{u}_n^B + \tau_{tn}^B\Delta\dot{u}_t^B)\end{aligned} \tag{27}$$

Note that, even though the strain rates approach infinity as the element thickness $\delta$ approaches zero, the strain rates times the element area are well defined in Equations (21)–(26). Indeed, the latter merely describe the finite normal and tangential velocity jumps which are permitted across a velocity discontinuity.

In global co-ordinates the velocity jumps are given by

$$\begin{bmatrix} \Delta\dot{u}_t^A \\ \Delta\dot{u}_n^A \\ \Delta\dot{u}_t^B \\ \Delta\dot{u}_n^B \end{bmatrix} = \begin{bmatrix} -\mathbf{T}^{\mathsf{T}} & \mathbf{0} & \mathbf{0} & \mathbf{T}^{\mathsf{T}} & \mathbf{0} & \mathbf{0} \\ \mathbf{0} & \mathbf{0} & -\mathbf{T}^{\mathsf{T}} & \mathbf{0} & \mathbf{T}^{\mathsf{T}} & \mathbf{0} \end{bmatrix} \dot{\mathbf{u}} \tag{28}$$

where

$$\dot{\mathbf{u}} = [\dot{u}_x^1,\ \dot{u}_y^1,\ \ldots,\ \dot{u}_y^6]^{\mathsf{T}} \tag{29}$$

and $\mathbf{T}$ is the standard transformation matrix

$$\mathbf{T} = \begin{bmatrix} \cos\theta & -\sin\theta \\ \sin\theta & \cos\theta \end{bmatrix} \tag{30}$$

For a two-element mesh with one discontinuity, as shown in Figure 3, the weak form of the equilibrium equations can then be written as

$$\begin{bmatrix} \mathbf{B}_1^{\mathsf{T}} & \mathbf{0} \\ \mathbf{0} & \mathbf{B}_2^{\mathsf{T}} \end{bmatrix} \begin{bmatrix} \boldsymbol{\sigma}_1 \\ \boldsymbol{\sigma}_2 \end{bmatrix} + \mathbf{S}^{\mathsf{T}}\boldsymbol{\rho} = \alpha\mathbf{p} \tag{31}$$

where

$$\mathbf{S} = \begin{bmatrix} -\mathbf{T}^{\mathsf{T}} & \mathbf{0} & \mathbf{0} & \mathbf{T}^{\mathsf{T}} & \mathbf{0} & \mathbf{0} \\ \mathbf{0} & \mathbf{0} & -\mathbf{T}^{\mathsf{T}} & \mathbf{0} & \mathbf{T}^{\mathsf{T}} & \mathbf{0} \end{bmatrix} \tag{32}$$

 

and

$$\boldsymbol{\rho} = \tfrac{1}{2} L[\tau_{tn}^{A},\ \ \sigma_{n}^{A},\ \ \tau_{tn}^{B},\ \ \sigma_{n}^{B}]^{\mathsf{T}} \tag{33}$$

*4.2. Discontinuity yield conditions*

For the discontinuities, yield conditions are applied as

$$f(\sigma_t, \sigma_n, \tau_{tn}) \leqslant 0 \tag{34}$$

By means of the associated flow rule and the fact that $\dot{\varepsilon}_t = 0$, the normal stress $\sigma_t$ can be eliminated. The associated flow reads

$$\dot{\varepsilon}_t = \dot{\lambda} \frac{\partial f}{\partial \sigma_t} = 0 \tag{35}$$

If we assume that $\dot{\lambda} > 0$, we can express $\sigma_t$ as a function of $\sigma_n$ and $\tau_{tn}$ by the condition that $\partial f / \partial \sigma_t = 0$ so that the yield condition (34) simplifies to

$$\hat{f}(\sigma_n, \tau_{tn}) = \hat{f}(\hat{\boldsymbol{\sigma}}) \leqslant 0 \tag{36}$$

where $\hat{\boldsymbol{\sigma}} = [\sigma_n, \tau_{tn}]^{\mathsf{T}}$. If $\dot{\lambda} = 0$ so that yielding does not occur, (36) can still be imposed since it will never be more restrictive than (34), i.e. it is always on the unsafe side to assume that $\dot{\lambda} > 0$.

*4.3. Discontinuous stress-based upper bound optimization problem*

Using the equilibrium equations (31) and the yield conditions (36), the $\alpha \rightarrow$ max load optimization problem corresponding to the two-element patch with a single discontinuity shown in Figure 3, can be written as

$$\begin{aligned}
&\text{maximize} \quad \alpha \\
&\text{subject to} \quad \begin{bmatrix} \mathbf{B}_1^{\mathsf{T}} & \mathbf{0} \\ \mathbf{0} & \mathbf{B}_2^{\mathsf{T}} \end{bmatrix} \begin{bmatrix} \boldsymbol{\sigma}_1 \\ \boldsymbol{\sigma}_2 \end{bmatrix} + \mathbf{S}^{\mathsf{T}} \boldsymbol{\rho} = \alpha \mathbf{p} \\
&\qquad\qquad f_1(\boldsymbol{\sigma}_1) \leqslant 0 \\
&\qquad\qquad f_2(\boldsymbol{\sigma}_2) \leqslant 0 \\
&\qquad\qquad \hat{f}_A(\hat{\boldsymbol{\sigma}}_A) \leqslant 0 \\
&\qquad\qquad \hat{f}_B(\hat{\boldsymbol{\sigma}}_B) \leqslant 0
\end{aligned} \tag{37}$$

Note that the simplification of the yield inequalities by elimination of $\sigma_t$ is not strictly necessary and has only been carried out for the purpose of comparing the new upper bound formulation with the traditional formulation where the velocities and plastic multipliers are used directly. This means that the last two inequalities, $\hat{f}_A(\hat{\boldsymbol{\sigma}}_A) \leqslant 0$ and $\hat{f}_B(\hat{\boldsymbol{\sigma}}_B) \leqslant 0$, can be replaced by $f_A(\boldsymbol{\sigma}_A) \leqslant 0$ and $f_B(\boldsymbol{\sigma}_B) \leqslant 0$ without any loss of generality. The fact that we can impose yield conditions of type (34) directly is one of the key advantages of the new formulation as no distinction needs to be made between continuum and discontinuity triangles.

 

*4.3.1. Discontinuous velocity-based upper bound optimization problem.* Consider the dual to (37), which is given by

$$\begin{aligned}
&\text{minimize} \quad \dot{\bar{\lambda}}_1 \nabla f_1^{\mathsf{T}} \boldsymbol{\sigma}_1^* + \dot{\bar{\lambda}}_2 \nabla f_2^{\mathsf{T}} \boldsymbol{\sigma}_2^* + \dot{\bar{\kappa}}_A \nabla \hat{f}_A^{\mathsf{T}} \hat{\boldsymbol{\sigma}}_A^* + \dot{\bar{\kappa}}_B \nabla \hat{f}_B^{\mathsf{T}} \hat{\boldsymbol{\sigma}}_B^* \\
&\text{subject to} \quad \begin{bmatrix} \mathbf{B}_1 & \mathbf{0} \\ \mathbf{0} & \mathbf{B}_2 \end{bmatrix} \begin{bmatrix} \mathbf{u}_1 \\ \mathbf{u}_2 \end{bmatrix} = \begin{bmatrix} \nabla f_1 & 0 \\ 0 & \nabla f_2 \end{bmatrix} \begin{bmatrix} \dot{\bar{\lambda}}_1 \\ \dot{\bar{\lambda}}_2 \end{bmatrix} \\
&\qquad\qquad \mathbf{S}\dot{\mathbf{u}} = \mathbf{C}\dot{\bar{\boldsymbol{\kappa}}} \\
&\qquad\qquad \mathbf{p}^{\mathsf{T}}\dot{\mathbf{u}} = 1 \\
&\qquad\qquad \dot{\bar{\boldsymbol{\lambda}}} \geqslant \mathbf{0}, \quad \dot{\bar{\boldsymbol{\kappa}}} \geqslant \mathbf{0}
\end{aligned} \tag{38}$$

where

$$\mathbf{C} = \begin{bmatrix} \nabla \hat{f}_A & \mathbf{0} \\ \mathbf{0} & \nabla \hat{f}_B \end{bmatrix} \tag{39}$$

and $\mathbf{S}$ is given by (32). Compared to the standard continuous FE formulation there are two changes. Firstly, an additional internal rate of dissipation stemming from the discontinuities appears in the objective function. In this connection two additional plastic multipliers $\dot{\bar{\boldsymbol{\kappa}}}$ have been introduced. Secondly, flow rules for the discontinuities are expressed through additional compatibility constraints. All constraints are imposed 'exactly', i.e. without compromising the requirements of the upper bound theorem, and the resulting value of the internal rate of dissipation, which is equal to $\alpha$ in (37), will therefore be an upper bound on the exact solution.

For the important special case of Mohr–Coulomb plasticity it can be shown, see Appendix A, that (37) is the dual of the velocity-based formulation of Sloan and Kleeman [9]. The stress-based problem is, however, much more convenient as general yield criteria are easily applied and the formulation can be extended to three dimensions in a straightforward manner.

### *4.4. Generalization to three dimensions and arbitrary yield criteria*

For the two-dimensional case, the choice of a local discontinuity co-ordinate system is useful. In three dimensions and for arbitrary yield criteria, however, it is more practical to refer to the global co-ordinate system.

The equilibrium matrices are most easily derived in terms of area co-ordinates. For a two-dimensional triangular element with vertices $(x_\alpha, y_\alpha)$, $\alpha = 1, 2, 3$, we have

$$\mathbf{B} = \int_V \mathbf{L}\mathbf{N}\,\mathrm{d}V = \frac{1}{2} \begin{bmatrix} y_2 - y_3 & 0 & y_3 - y_1 & 0 & y_1 - y_2 & 0 \\ 0 & x_3 - x_2 & 0 & x_1 - x_3 & 0 & x_2 - x_1 \\ x_3 - x_2 & y_2 - y_3 & x_1 - x_3 & y_3 - y_1 & x_2 - x_1 & y_1 - y_2 \end{bmatrix} \tag{40}$$

which is applicable to continuum elements as well as to discontinuity elements. Thus, the inclusion of kinematically admissible discontinuities only involves a modification of the node

 

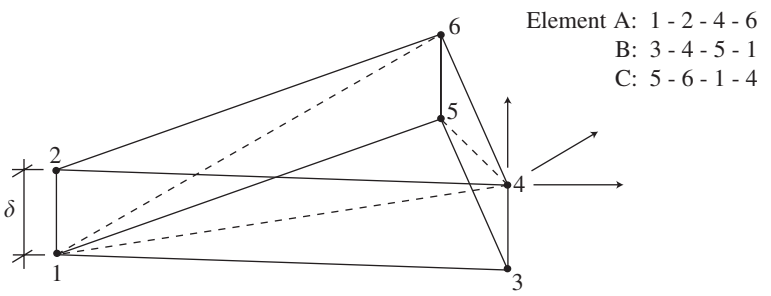


Figure 5. Three-dimensional discontinuity.

numbering, whereas the computation of the local equilibrium matrices is handled in exactly the same way as for the continuum elements.

In the three dimensional case the discontinuity plane is divided into three tetrahedra as shown in Figure 5. These each have a volume equal to $\frac{1}{3}\delta A$, where $A$ is the interface area. For each of these elements the equilibrium matrix can be computed in a manner analogous to the two-dimensional case.

The yield criteria are applied in exactly the same way as for the continuum elements. Since the state of stress is constant within each element, discontinuity elements are treated no differently to the continuum elements. Thus, the final problem can be written as

$$\begin{aligned} &\text{maximize} && \alpha \\ &\text{subject to} && \mathbf{B}^{\mathrm{T}}\boldsymbol{\sigma} = \alpha\mathbf{p} \\ & && \mathbf{f}(\boldsymbol{\sigma}) \leqslant 0 \end{aligned} \tag{41}$$

where $\mathbf{B}$ are $\mathbf{p}$ assembled by contributions from the individual elements (of which some may have zero volume) and the yield conditions are applied to each element.

## 5. EXAMPLES

We now analyse some classical stability problems to test the accuracy and efficiency of the new upper bound formulation. The cases considered involve the Tresca, Mohr–Coulomb, Drucker–Prager and Reinicke–Ralston yield criteria to cover both isotropic and anisotropic materials.

For each of the problems, moderate density structured meshes have been generated in order to give an objective comparison of the new formulation with conventional schemes. The formulations used for comparison include the upper bound formulations of Lyamin and Sloan [10] and Lyamin *et al.* [12], as well as the lower bound scheme of Lyamin and Sloan [13].

In the case of Mohr–Coulomb plasticity the smoothed approximation suggested by Abbo and Sloan [14] is used. In all cases the optimization problem resulting from the new upper bound formulation is solved by the algorithm described in Reference [13].

 

The CPU times quoted are for an AMD Athlon 2100+ processor operating under Windows XP Professional Edition. The compiler used was Visual Fortran Standard Edition 6.6 with full optimization.

### *5.1. Slope stability*

This is a classical soil stability problem with an accurate upper bound solution available to test the validity of the newly developed approach. The finite element mesh, boundary conditions and material properties adopted in the analysis, as well as the resultant velocity field and plasticity zones, are shown in Figure 6.

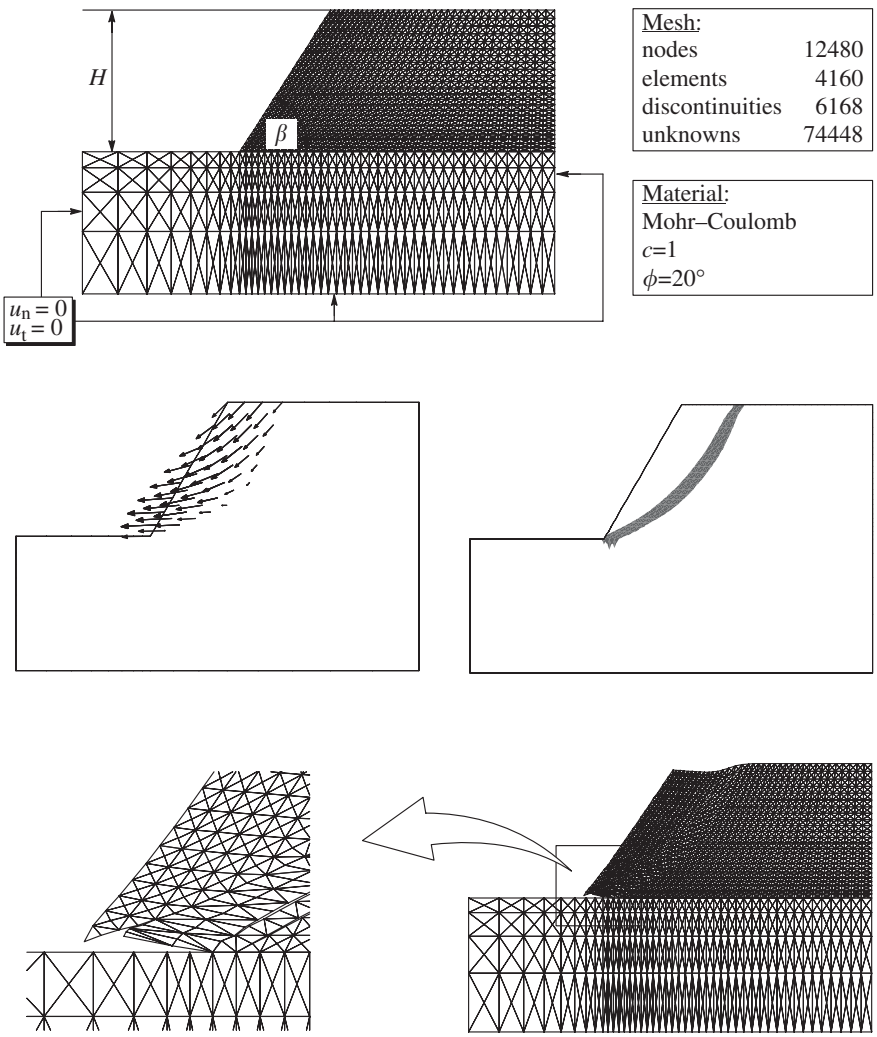


Figure 6. Slope stability—mesh, velocity field, plastic multiplier field and deformed mesh.

 

Table I. Upper and lower bounds for slope stability problem.

| Slope angle (°) | Lower bound Lyamin and Sloan [13] | Upper bound Chen [15] | Upper bound Lyamin and Sloan [10] | | | Upper bound Present | | |
|---|---|---|---|---|---|---|---|---|
| | $\gamma H/c$ | $\gamma H/c$ | $\gamma H/c$ | Iterations | CPU (s) | $\gamma H/c$ | Iterations | CPU (s) |
| 90 | 5.41 | 5.50 | 5.67 | 48(+13)* | 50 | 5.67 | 27 | 23 |
| 80 | 6.58 | 6.75 | 6.89 | 46(+13)* | 48 | 6.89 | 27 | 22 |
| 70 | 8.12 | 8.30 | 8.44 | 46(+13)* | 48 | 8.44 | 29 | 23 |
| 60 | 10.21 | 10.39 | 10.54 | 43(+13)* | 46 | 10.54 | 30 | 24 |
| 50 | 13.44 | 13.63 | 13.79 | 39(+13)* | 43 | 13.79 | 33 | 27 |

*Phase one iterations to obtain initial feasible point.

The results of the calculations for a range of slope angles are shown in Table I. As expected, the new formulation gives the same estimate of the collapse load as the upper bound formulation of Lyamin and Sloan [10]. These estimates are in good agreement with the analytical upper bound solution of Chen [15] as well as with the lower bound results computed using the procedure of Reference [13]. As discussed elsewhere in detail, see e.g. References [9, 10], this demonstrates that accurate upper bound solutions can be obtained with a moderate computational effort using low-order elements, provided that kinematically admissible discontinuities are included between adjacent elements.

As for the computational effort, the new formulation is roughly twice as efficient as the conventional one, although this feature is of course problem dependent. A noticeable difference is, however, that the conventional scheme requires the solution of a phase 1 problem to generate an initial feasible solution [10]. Such a solution is easily obtained with the new formulation by simply setting all stresses and the load multiplier equal to zero.

### *5.2. Ice sheet indentation*

The problem of indentation of an ice sheet, as shown in Figure 7, is of engineering interest because of its similarity to the crushing of ice sheets moving towards a vertical pier. The problem is basically three-dimensional with the thickness $t$ of the ice sheet and the size and shape of the indentor being the governing geometric parameters. If the indentor is assumed prismatic with a width $b$ as indicated in the figure, the problem may, depending on the ratio $b/t$, be idealized as a either a plane strain ($b/t = 0$) or a plane stress ($b/t = \infty$) problem. In the following these two cases will be analysed.

The strength of columnar-grained ice is anisotropic, sensitive to confining stress, and differs in tension and compression. A yield criterion capable of capturing these characteristics has been proposed by Reinicke and Ralston [16] as

$$f(\boldsymbol{\sigma}) = a_1[(\sigma_y - \sigma_z)^2 + (\sigma_z - \sigma_x)^2] + a_3(\sigma_x - \sigma_y)^2 + a_4(\tau_{yz}^2 + \tau_{zx}^2) + a_6\tau_{xy}^2 + a_7(\sigma_x + \sigma_y) + a_9\sigma_z - 1 = 0 \tag{42}$$

where $a_6 = 2(a_1 + 2a_3)$. From this general criterion, plane stress and plane strain criteria can be derived as, see Reference [17],

 

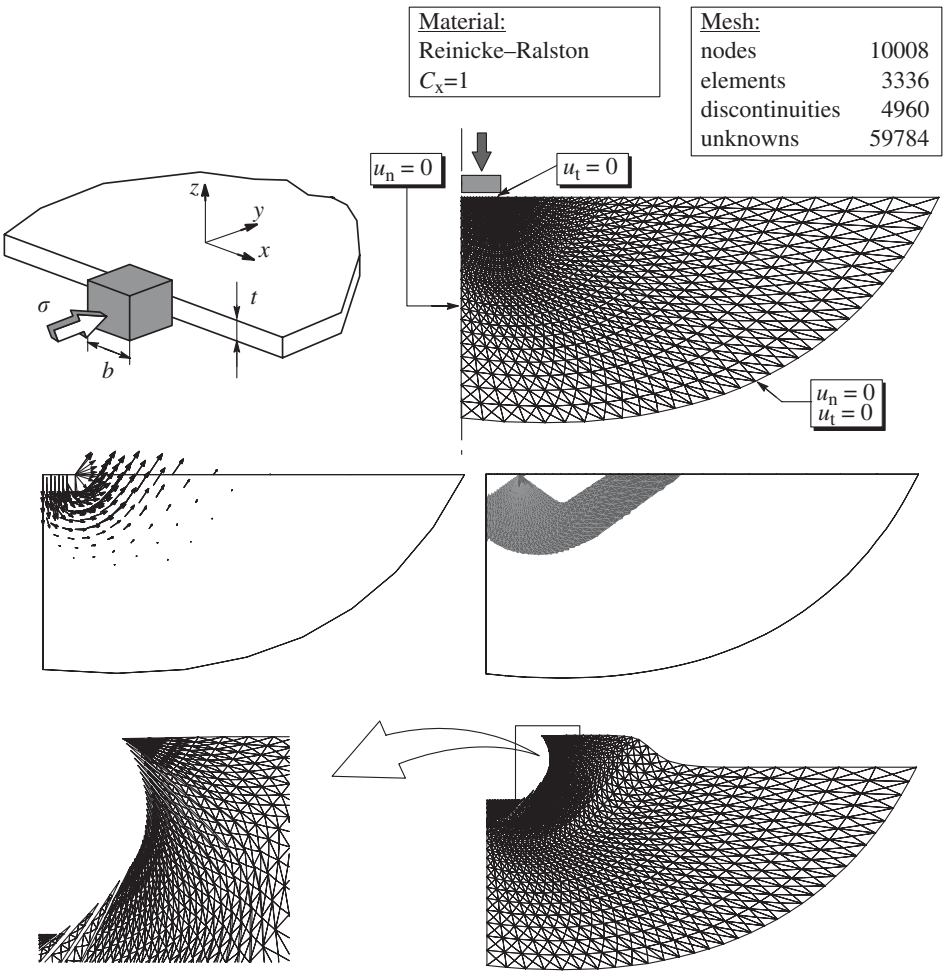


Figure 7. Ice sheet indentation—physical problem, mesh, velocity field, plastic multiplier field and deformed mesh.

Plane strain:

$$f(\boldsymbol{\sigma}) = a_6[\tfrac{1}{4}(\sigma_x - \sigma_y)^2 + \tau_{xy}^2] + \tfrac{1}{2}(2a_7 + a_9)(\sigma_x + \sigma_y) - (1 + \tfrac{1}{8}a_9^2/a_1) = 0$$

Plane stress:

$$f(\boldsymbol{\sigma}) = a_1(\sigma_x^2 + \sigma_y^2) + a_3(\sigma_x - \sigma_y)^2 + a_6\tau_{xy}^2 + a_7(\sigma_x + \sigma_y) - 1 = 0 \tag{43}$$

The kinematically admissible velocity discontinuities corresponding to these yield criteria are non-trivial. With the new formulation, however, the yield criteria are easily implemented in the general $\alpha \rightarrow$ max procedure (9).

 

Table II. Upper and lower bounds for ice sheet indentation example.

| Aspect ratio $b/t$ | Upper bound (Analytical [16]) | Upper bound (No discont.) | Lower bound (Numerical [13]) | Upper bound (Present) |
|---|---|---|---|---|
| 0 (plane strain) | 4.47 | 4.48 | 4.08 | 4.16 |
| $\infty$ (plane stress) | 3.38 | 3.41 | 3.11 | 3.16 |

Following the ice indentation experiments conducted by Ralston [18] the parameters $a_1$, $a_3$, $a_7$ and $a_9$ are taken as

$$a_1 = 1.77C_x^{-2}, \quad a_3 = 5.27C_x^{-2}, \quad a_7 = 6.04C_x^{-1}, \quad a_9 = -3.54C_x^{-1} \tag{44}$$

where $C_x$ is the in-plane unconfined compressive strength.

Table II shows the results of the analyses together with the analytical bounds of Reinicke and Ralston [16] and a lower bound solution using the formulation of Lyamin and Sloan [13] for a mesh similar to that shown in Figure 7. The computed upper bound solutions compare very well with the numerical lower bound solution, with the maximum difference being less than 2%, whereas the analytical upper bounds solution of Reinicke and Ralston [16] are approximately 7% higher than those computed numerically with the present discontinuous formulation. If no discontinuities are included in the mesh, a similar increase in the limit load is seen.

### *5.3. Conical excavation*

The stability of a conical excavation, as shown in Figure 8, is the 3D analogue to the slope stability problem considered in the first example. It is therefore interesting to verify not only the performance of new formulation in 3D case but also the difference between the two- and three-dimensional models of the same problem. To increase the accuracy of the computed stability factors, the symmetry inherent in the case of a conical excavation is fully exploited. Thus, only a 15° section is discretized as shown in Figure 8. This figure also shows the boundary conditions adopted in the analysis, the resultant plasticity zones (shaded area), and the deformation patterns.

The results of the analyses are shown in Table III together with upper and lower bounds using the methods described in References [10, 12, 13]. In two dimensions the Mohr–Coulomb criterion results in linear discontinuity flow rule constraints as given by (A8). In three dimensions, however, these conditions are non-linear and non-differentiable. With the original three-dimensional upper bound formulation of Lyamin and Sloan [10] the flow rule constraints were linearized conservatively to give rigorous bounds, whereas in Reference [12] the exact non-linear conditions were smoothed and imposed directly. The results reveal that the present upper bound formulation, depending on the particular geometry, is approximately two to four times as efficient as that of Lyamin *et al*. [12]. In Reference [12] the discontinuity flow rule constraints were smoothed to within a very tight tolerance and it is not surprising that the two sets of upper bound results differ only slightly. Compared to the original formulation [10], where linearized flow rule constraints were imposed, the present formulation is equally efficient in terms of computation time, but the results are slightly better—for $\beta = 90°$ the improvement is approximately 3%. It should be noted that the new upper bounds differ by only 5% from the lower bounds computed using the same mesh, thus confirming the feasibility of the method.

 

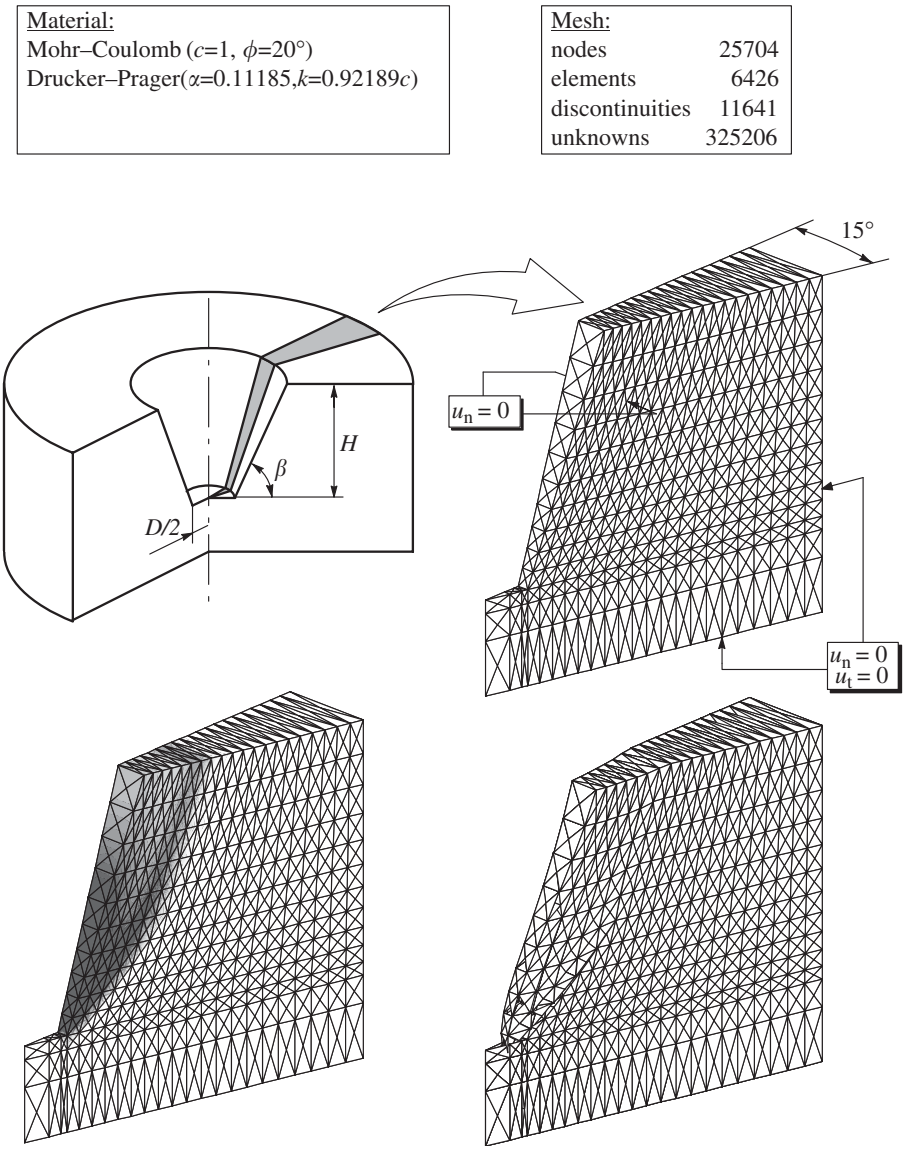


Figure 8. Conical excavation—physical problem, mesh, plastic multiplier field and deformed mesh.

Perhaps the most obvious advantage of the new discontinuous upper bound formulation is the ability to treat arbitrary yield conditions in two and three spatial dimensions. The last example illustrates this by the computation of the limit loads for the same example as described in the above, but now using the Drucker–Prager criterion, which is given by

$$f(I_1, J_2) = \alpha I_1 + \sqrt{J_2} - k \leqslant 0 \tag{45}$$

 

Table III. Upper and lower bounds for conical excavation example using Mohr–Coulomb criterion.

| Angle $\beta$ (°) | Lower bound Lyamin and Sloan [13] | Upper bound Lyamin and Sloan [10] | | Upper bound Lyamin *et al.* [12] | | Upper bound Present | | |
|---|---|---|---|---|---|---|---|---|
| | $\gamma H/c$ | $\gamma H/c$ | CPU (h:min) | $\gamma H/c$ | CPU (h:min) | $\gamma H/c$ | CPU (h:min) | Iterations |
| 50 | 26.10 | 27.99 | 0:40 | 27.76 | 1:12 | 27.72 | 0:52 | 237 |
| 60 | 21.03 | 22.54 | 0:39 | 22.37 | 2:08 | 22.34 | 0:45 | 219 |
| 70 | 18.15 | 19.55 | 0:32 | 19.28 | 1:44 | 19.25 | 0:43 | 205 |
| 80 | 16.64 | 17.96 | 0:37 | 17.57 | 2:20 | 17.55 | 0:38 | 192 |
| 90 | 16.18 | 17.63 | 0:42 | 17.11 | 3:50 | 17.09 | 0:41 | 207 |

Table IV. Upper and lower bounds for conical excavation example using Drucker–Prager yield criterion.

| Angle $\beta$ (°) | Lower bound Lyamin and Sloan [13] | | | Upper bound Present | | |
|---|---|---|---|---|---|---|
| | $\gamma H/k$ | Iterations | CPU (min:s) | $\gamma H/k$ | Iterations | CPU (min:s) |
| 50 | 26.26 | 23 | 22:06 | 27.94 | 39 | 8:52 |
| 60 | 21.48 | 22 | 21:30 | 22.56 | 38 | 8:06 |
| 70 | 18.65 | 23 | 20:15 | 19.59 | 34 | 7:23 |
| 80 | 17.12 | 22 | 21:15 | 17.92 | 30 | 6:18 |
| 90 | 16.63 | 20 | 20:06 | 17.46 | 30 | 6:12 |

In the following, the parameters $\alpha$ and $k$ are chosen as

$$\alpha = \frac{\tan\phi}{\sqrt{9 + 12\tan^2\phi}}, \quad k = \frac{3c}{\sqrt{9 + 12\tan^2\phi}} \tag{46}$$

so that the Mohr–Coulomb and Drucker–Prager yield surfaces match each other in the plane strain case. As before, we use $\phi = 20°$ which gives

$$\alpha = 0.11185, \quad k = 0.92189c \tag{47}$$

Upper and lower bound results, both computed for the mesh shown in Figure 8, are given in Table IV. These indicate that the stability factors obtained with the Drucker–Prager criterion are quite similar to those obtained with the Mohr–Coulomb criterion. This conclusion, however, is not general but holds only for this particular problem. As can be seen, significantly fewer iterations are required with the 3D Drucker–Prager criterion than with the Mohr–Coulomb criterion. This is not surprising in view of the relative smoothness of the former over the latter criterion.

Quite surprisingly, the upper bound formulation requires approximately 1.5–2 times as many iterations as the lower bound formulation, though the latter involves roughly four times as many variables. This trend seems to be consistent, at least once the problem reaches a certain size, and has also been observed using the procedure described in Reference [19], both for problems involving non-linear yield criteria and for problems where these were linearized.

 

## 6. CONCLUSIONS

A new discontinuous upper bound formulation for the limit analysis of two- and three-dimensional solids has been presented. In contrast to previous formulations, the new method is applicable to general yield criteria which is demonstrated through a number of examples. Furthermore, kinematically admissible discontinuities are included in a straightforward manner and the method is generally much easier to implement than existing methods.

## APPENDIX A: PLANE STRAIN MOHR–COULOMB PLASTICITY

As a special case of the treatment of velocity discontinuities plane strain Mohr–Coulomb plasticity is considered. The yield condition is here given by

$$f(\sigma_t, \sigma_n, \tau_{tn}) = \sqrt{(\sigma_t - \sigma_n)^2 + 4\tau_{tn}^2} - (2c\cos\phi - (\sigma_t + \sigma_n)\sin\phi) \leqslant 0 \tag{A1}$$

Using the fact that $\dot{\varepsilon}_t = 0$ together with the associated flow rule gives

$$\dot{\varepsilon}_t = \dot{\lambda}\frac{\partial f}{\partial \sigma_t} = 0 \Rightarrow \sigma_t = \sigma_n - 2|\tau_{tn}|\tan\phi \tag{A2}$$

Inserting this into the yield function gives the relation

$$|\tau_{tn}| \leqslant c - \sigma_n \tan\phi \tag{A3}$$

which is then the yield criterion for the discontinuity elements. In matrix form the yield constraints for the discontinuity elements are given by

$$\mathbf{C}^{\mathsf{T}}\boldsymbol{\rho} \leqslant \mathbf{c}_0 \tag{A4}$$

where

$$\mathbf{C}^{\mathsf{T}} = \begin{bmatrix} 1 & \tan\phi & & \\ -1 & \tan\phi & & \\ & & 1 & \tan\phi \\ & & -1 & \tan\phi \end{bmatrix}, \quad \mathbf{c}_0 = L\begin{bmatrix} \frac{1}{2}c \\ \frac{1}{2}c \\ \frac{1}{2}c \\ \frac{1}{2}c \end{bmatrix} \tag{A5}$$

Using the equilibrium equations (31) and the yield conditions (A4), the $\alpha \rightarrow$ max load optimization problem corresponding to the two-element patch with a single discontinuity shown in Figure 3, can be written as

$$\begin{aligned} &\text{maximize} \quad \alpha \\ &\text{subject to} \quad \begin{bmatrix} \mathbf{B}_1^{\mathsf{T}} & \mathbf{0} \\ \mathbf{0} & \mathbf{B}_2^{\mathsf{T}} \end{bmatrix}\begin{bmatrix} \boldsymbol{\sigma}_1 \\ \boldsymbol{\sigma}_2 \end{bmatrix} + \mathbf{S}^{\mathsf{T}}\boldsymbol{\rho} = \alpha\mathbf{p} \end{aligned} \tag{A6}$$

 

$$f_1(\boldsymbol{\sigma}_1) \leqslant 0$$

$$f_2(\boldsymbol{\sigma}_2) \leqslant 0$$

$$\mathbf{C}^{\mathrm{T}}\boldsymbol{\rho} \leqslant \mathbf{c}_0$$

The dual to (A6) is given by

$$\begin{aligned}
&\text{minimize} \quad \dot{\bar{\lambda}}_1 \nabla f_1^{\mathrm{T}} \sigma_1^* + \dot{\bar{\lambda}}_2 \nabla f_2^{\mathrm{T}} \sigma_2^* + \mathbf{c}_0^{\mathrm{T}} \dot{\bar{\boldsymbol{\kappa}}} \\
&\text{subject to} \quad \begin{bmatrix} \mathbf{B}_1 & \mathbf{0} \\ \mathbf{0} & \mathbf{B}_2 \end{bmatrix} \begin{bmatrix} \mathbf{u}_1 \\ \mathbf{u}_2 \end{bmatrix} = \begin{bmatrix} \nabla f_1 & 0 \\ 0 & \nabla f_2 \end{bmatrix} \begin{bmatrix} \dot{\bar{\lambda}}_1 \\ \dot{\bar{\lambda}}_2 \end{bmatrix} \\
&\mathbf{S}\dot{\mathbf{u}} = \mathbf{C}\dot{\bar{\boldsymbol{\kappa}}} \\
&\mathbf{p}^{\mathrm{T}}\dot{\mathbf{u}} = 1 \\
&\dot{\bar{\boldsymbol{\lambda}}} \geqslant \mathbf{0}, \quad \dot{\bar{\boldsymbol{\kappa}}} \geqslant \mathbf{0}
\end{aligned} \tag{A7}$$

The discontinuity flow rules are here given by, see Figure A1,

$$\underbrace{\begin{bmatrix} \Delta\dot{u}_t^A \\ \Delta\dot{u}_n^A \\ \Delta\dot{u}_t^B \\ \Delta\dot{u}_n^B \end{bmatrix}}_{\mathbf{S}\dot{\mathbf{u}}} = \underbrace{\begin{bmatrix} 1 & -1 & & \\ \tan\phi & \tan\phi & & \\ & & 1 & -1 \\ & & \tan\phi & \tan\phi \end{bmatrix}}_{\mathbf{C}} \underbrace{\begin{bmatrix} \dot{\bar{\kappa}}_A^+ \\ \dot{\bar{\kappa}}_A^- \\ \dot{\bar{\kappa}}_B^+ \\ \dot{\bar{\kappa}}_B^- \end{bmatrix}}_{\dot{\bar{\boldsymbol{\kappa}}}} \tag{A8}$$

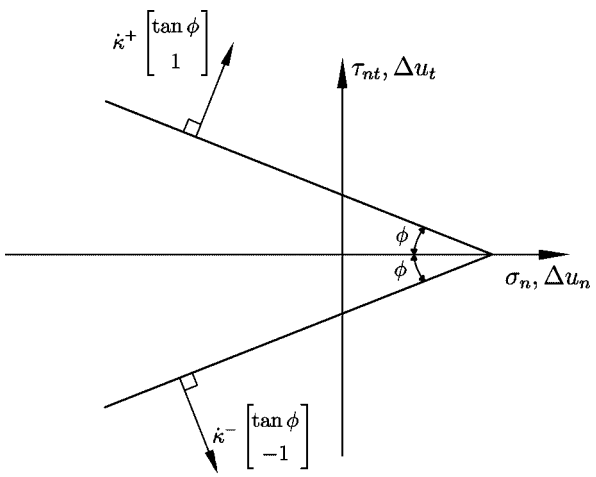


Figure A1. Flow rule for discontinuities.

 

where **S** is defined in (32). Problem (A7) is identical to that derived by Sloan and Kleeman [9], provided that the cohesion is constant within the individual elements and discontinuities, and describes a traditional upper bound formulation.

## REFERENCES


1. Nguyen Quoc Son, Radenkovic D. La dualité des théorémes limites pour une structure rigid plastic standard. *Archives of Mechanics* 1972; **24**:991–998.
2. Gao DY. On the complementary bounding theorem for limit analysis. *International Journal of Solids and Structures* 1988; **24**:545–556.
3. Anderheggen E, Knöpfel H. Finite element limit analysis using linear programming. *International Journal of Solids and Structures* 1972; **8**:1413–1431.
4. Borges LA, Zouain N, Huespe AE. A non-linear optimization procedure for limit analysis. *European Journal of Mechanics – A/Solids* 1996; **15**(3):487–512.
5. Nash SG, Sofer A. *Linear and Nonlinear Programming*. McGraw-Hill: New York, 1996.
6. Nagtegaal JC, Parks DM, Rice JR. On numerically accurate finite element solutions in the fully plastic range. *Computer Methods in Applied Mechanics and Engineering* 1974; **4**:153–178.
7. Wells GN, Sluys LJ, de Borst R. A *p*-adaptive scheme for overcoming volumetric locking during plastic flow. *Computer Methods in Applied Mechanics and Engineering* 2002; **191**:3153–3164.
8. Sloan SW, Randolph MF. Numerical prediction of collapse loads using finite element methods. *International Journal for Numerical and Analytical Methods in Geomechanics* 1982; **6**:47–76.
9. Sloan SW, Kleeman PW. Upper bound limit analysis using discontinuous velocity fields. *Computer Methods in Applied Mechanics and Engineering* 1995; **127**:293–314.
10. Lyamin AV, Sloan SW. Upper bound limit analysis using linear finite elements and non-linear programming. *International Journal for Numerical and Analytical Methods in Geomechanics* 2002; **26**:181–216.
11. Zienkiewicz OC, Taylor RL. *The Finite Element Method*. Butterworth-Heinemann: Oxford, 2000.
12. Lyamin AV, Sloan SW, Hjiaj M. Different approaches to introduction of velocity discontinuities in upper bound limit analysis. In *Book of Abstracts Fifth Euromech Solid Mechanics Conference*, Aifantis EC (ed.). Thessaloniki: Greece, 2003.
13. Lyamin AV, Sloan SW. Lower bound limit analysis using non-linear programming. *International Journal for Numerical Methods in Engineering* 2002; **55**:573–611.
14. Abbo AJ, Sloan SW. A smoothed hyperbolic approximation to the Mohr–Coulomb yield criterion. *Computers and Structures* 1995; **54**:427–441.
15. Chen WF, Liu XL. *Limit Analysis in Soil Mechanics*. Elsevier Science Publishers B.V.: Amsterdam, 1990.
16. Reinicke KM, Ralston TD. Plastic limit analysis with and anisotropic parabolic yield function. *International Journal for Rock Mechanics and Mining Sciences* 1977; **14**:147–154.
17. Chen WF, Han DJ. *Plasticity for Structural Engineers*. Springer: New York, 1988.
18. Ralston KM. An analysis of ice sheet indentation. In *Fourth International Symposium on Ice Problems*. International Association for Hydraulic Research: Luleå, Sweden, 1978; 13–31.
19. Krabbenhoft K, Damkilde L. A general nonlinear optimization algorithm for lower bound limit analysis. *International Journal for Numerical Methods in Engineering* 2003; **56**:165–184.


 